Modeling Studies of Low-Temperature Aerobic NO_x Reduction by a Sequence of LNT-SCR Catalysts

Arun S Kota, Dan Luss and Vemuri Balakotaiah
Dept. of Chemical and Biomolecular Engineering, University of Houston, Houston, TX 77204

DOI 10.1002/aic.14171
Published online August 2, 2013 in Wiley Online Library (wileyonlinelibrary.com)

The relationship between fuel penalty and precious metal loading in coupled LNT—SCR systems for NO_x reduction at low temperatures is determined. Simulations of adiabatic, aerobic NO_x reduction determine the impact of catalyst architecture, precious metal loading, cycle time, catalyst length and the support material. These revealed that (a) high NO_x conversion can be achieved for a given precious metal loading at low temperatures (510 K) with about 0.3% fuel penalty, (b) shortened cycle time and increased pulse duty reduce the overall NO_x slip from the coupled catalyst and lead to significant improvement in the NO_x conversion, (c) alternate arrangement of the LNT/SCR catalysts increases the NO_x conversion, (d) a monotonic decreasing PGM loading in LNT leads to higher NO_x conversion compared to uniform loading, (e) for a fixed catalyst volume, there is an optimal aspect ratio that maximizes the nonisothermal effect, and (f) metal based monolith supports improve NO_x conversion. © 2013 American Institute of Chemical Engineers *AIChE J*, 59: 3421-3431, 2013

Keywords: catalysis, environmental engineering, reactor analysis

Introduction

Diesel engines operate with A/F ratios around 16:1 to 17:1 and generate emissions including NO_x and particulate matter. It is difficult to reduce the NO_x in this oxygen rich environment. Leading technologies like lean NO_x Traps (LNT) and selective catalytic reduction (SCR) enable lean NO_x reduction that meets stringent emission regulations.

Lean NO_x trap (LNT) is used to periodically store and then reduce NO_x in an alternate lean and rich cyclic operation. LNT catalyst consists of precious group metals (Pt, Rh, etc.) and oxides of alkaline earth metal (Ba, K), supported on a high-surface area metal oxide carrier like Al_2O_3, MgO, etc. The most common LNT catalyst is $Pt/BaO/Al_2O_3$.[1–3] NO_x is stored on the trapping material (BaO) during the lean period. It is subsequently purged by a rich feed (containing reducing agents like H_2, hydrocarbons, etc) to form N_2, NH_3 and H_2O. The precious metal catalyst (Pt) used in the LNT is expensive and it is desirable to reduce the Pt loading while achieving high conversions.

Urea has been commercially used to produce NH_3 to enable the selective catalytic reduction of NO_x. The urea feed leads to high-operation cost, freezing during cold weather[4] and control problems. One can avoid the need for the complex NH_3 feed and decrease the NO_x emissions from the LNT using a combination of the LNT and SCR catalytic systems,[5,6] where the NH_3 generated in the LNT is used in the SCR catalyst downstream to reduce the NO_x. This combination offers several advantages like reducing the precious metal cost, reduced NH_3 slip and efficient NO_x reduction. Lietti et al.[7] and Seo et al.[8] studied NO_x reduction by a sequential pair of LNT and SCR catalysts. They reported a pronounced improvement in the NO_x removal efficiency especially at low temperatures (<473 K) at which a considerable NH_3 slip from the LNT catalyst occurs. Researchers at Ford Motor Co.[9,10] showed that a sequential LNT and SCR catalytic system enhanced the NO_x conversion. Kota et al.[11] studied the impact of operating conditions and architectural configurations of sequential LNT—SCR catalytic systems under isothermal conditions.

In practice, the LNT or the SCR systems do not operate isothermally, while most laboratory studies are of isothermal systems. Only a few studies are of the adiabatic operation of the LNT—SCR system. Koltsakis et al.[12] used a model to determine the dynamic behavior of the sequential and layered arrangements of LNT—SCR catalysts under adiabatic conditions. Similarly, Chatterjee et al.[13] used both modeling and experiments to study the performance of the combined LNT—SCR system under nonisothermal conditions. No attempt was made in these studies to optimize the operation of the coupled LNT—SCR system. It is intuitively obvious that the nonisothermal effect during the aerobic operation enhances the NO_x conversion over that of anaerobic operation which is nearly isothermal. However, it is not obvious what is the fuel penalty needed to achieve a desired NO_x conversion, especially at low-temperature operation of these systems. We report here a study of the dynamic behavior and the impact of the operating conditions on the performance of the sequential, adiabatic LNT—SCR catalytic system under aerobic and anaerobic conditions. The goal is to provide guidance about the optimal operation.

Additional Supporting Information may be found in the online version of this article.

Correspondence concerning this article should be addressed to V. Balakotaiah at bala@uh.edu (VB), and D. Luss at dluss@uh.edu (DL).

Mathematical Model Development

Model of LNT and SCR catalysts

The dynamic behavior of a sequence of LNT and SCR catalysts during a periodic lean and rich feed is investigated using species and energy balances. These account for the impact of washcoat diffusion on the reaction rate. The model assumes that (1) the physical properties of the exhaust gas are unaffected by composition changes, (2) the axial dispersion in gas phase is negligible compared to convection, (3) the flow in the monolith channels is laminar and fully developed, and (4) the catalyst system operates under adiabatic conditions.

The fluid phase balance of the dimensionless mixed-cup mole fraction of species j, $X_{j,m}$ is

$$\frac{\partial X_{j,m}}{\partial t} = -\bar{u}\frac{\partial X_{j,m}}{\partial z} - \frac{k_c(j,z)}{R_\Omega}\left(X_{j,m} - X_{j,wc}\right) \tag{1}$$

The subscript j represents the species $(j = NO, NO_2, O_2, H_2, NH_3, H_2O)$, $\bar{u}$ is the average velocity, the position dependent mass transfer coefficient $k_c(j,z) = 4R_\Omega / D_{m,j} Sh_e(z)$ accounts for the transverse gradients in the gas phase, R_Ω is the effective transverse length scale, $D_{m,j}$ is the diffusivity of species j in the bulk fluid, $Sh_e(z)$ is the position dependent external Sherwood number.[14]

In the prior study[11] it has been shown that neglecting washcoat diffusion results in an over estimation of the NO_x conversion in the sequential LNT and SCR catalysts. Therefore, we consider here the full diffusion-reaction model inside the washcoat. The washcoat balances are

$$\varepsilon_{wc}\frac{\partial X_{j,wc}}{\partial t} = D_{e,wc}\frac{\partial^2 X_{j,wc}}{\partial y^2} - \frac{\sum_{l=1}^{rxn}\left(v_{l,j}R_{V,l}\left(\theta, X_{j,wc}\right) - R_{ads,j} + R_{des,j}\right)}{C_{Tm}} \tag{2}$$

where ε_{wc} is the washcoat porosity, $D_{e,wc}$ is the effective species diffusivity inside the washcoat, C_{Tm} the total molar concentration, $X_{j,wc}$ is the mole fraction of species j in the washcoat, θ is the coverage of adsorbed species on the surface, $R_{V,l}\left(\theta, X_{j,wc}\right)$ is the volumetric rate of the reaction l, $R_{ads,j}$ is the adsorption rate, and $R_{des,j}$ is the desorption rate of species j from the washcoat. The effective diffusivity of species in the washcoat $(D_{e,wc})$ is calculated using the Knudsen diffusivity[15]

$$D_{e,wc} = \frac{\varepsilon_{wc}}{\tau} 97a\left(\frac{T_s}{M_m}\right)^{0.5} \tag{3}$$

where, washcoat porosity $(\varepsilon_{wc})$is 0.41, the tortuosity factor $\tau \approx 8$, the average pore radius (a) is $\sim 10^{-8}$ m, T_s is the monolith temperature, and M_m the molecular weight of the species. The gas phase diffusivities are calculated using Lennard-Jones parameters and are given in Table 6.

The surface coverage of the adsorbed species on the LNT catalyst is described by

$$C_{BaO}(f,s)\frac{\partial \theta_v(f,s)}{\partial t} = \sum_{l=1}^{rxn} v_{l,BaO(f,s)} R_{V,l}\left(\theta, X_{j,wc}\right) \tag{4}$$

$$C_X\frac{\partial X_{j,X}}{\partial t} = R_{ads,j} - R_{des,j} \tag{5}$$

$C_{BaO}(f,s)$ is the concentration of fast or slow BaO storage sites which are defined by their proximity to Pt. Storage sites that are in close proximity are called "fast" sites and those farther away are called "slow" sites. Here, $\theta_v(f,s)$ is the fractional coverage of the fast or slow sites in the washcoat, v_l is the stoichiometric coefficient in the reaction $\theta_{j,X}$, is the coverage on Al_2O_3 sites by NH_3 and H_2O, and C_X is the total concentration of adsorption sites on Al_2O_3 for NH_3 and H_2O. Fractional coverage of the adsorbed species on the SCR catalyst surface is described by

$$C_S\frac{\partial \theta_{j,s}}{\partial t} = \sum_{m=1}^{rxn} v_{m,j} R_{V,m}\left(\theta, X_{j,wc}\right) \tag{6}$$

where, $\theta_{j,s}$ is the fractional coverage of NH_3 on the zeolite, C_S is the concentration of adsorption sites on the Cu-ZSM5 catalyst,$v_{m,j}$ is the stoichiometric coefficient of species j in reaction m, and $R_{V,m}(\theta, X_{wc})$ is the reaction rate.

The gas phase and washcoated support energy balances are

$$\rho_f C_{p,f}\frac{\partial T_f}{\partial t} = -\bar{u}\rho_f C_{p,f}\frac{\partial T_f}{\partial z} - \frac{h_f}{R_\Omega}\left(T_f - T_s\right) \tag{7}$$

$$\delta_s\rho_s C_{p,s}\frac{\partial T_s}{\partial t} = \delta_s k_s\frac{\partial^2 T_s}{\partial z^2} - h_f\left(T_s - T_f\right) + \delta_{wc}\sum_{l=1}^{r}\left(-\Delta H_{R,l}\right) \times R_{V,l}\left(X_{j,wc}, \theta\right) \tag{8}$$

where, ρ_f is the density of gas (kg/m^3), $C_{p,f}$ the specific heat capacity of gas (J/(kg.K)), the heat transfer coefficient (W/m^2 K), T_f the gas-phase temperature, T_s the solid phase (washcoat and the channel wall) temperature $\delta_s\rho_s C_{p,s} = \delta_{wc}\rho_{wc}C_{p,wc} + \delta_{wall}\rho_{wall}C_{p,wall}$ accounts for the effective solid phase heat capacity, and $\delta_s k_s = \delta_{wc}k_{wc} + \delta_{wall}k_{wall}$ for the effective solid phase thermal conductivity. The values of the geometric parameters are reported in Table 1.

The transient model includes the following initial and boundary conditions,

$$X_{j,m}(z, t=0) = 0 \tag{9}$$

$$X_{j,wc}(y, z, t=0) = 0 \tag{10}$$

$$\theta_j(z, t=0) = \theta_{jo} = 0 \tag{11}$$

$$T_f(z, t=0) = T_s(z, t=0) = T_{\text{initial}}(z) \tag{12}$$

$$k_c(j,z)\left(X_{j,m}(y,z,t) - X_{j,wc}(y,z,t)\right) = -D_{e,wc}\frac{\partial X_{j,wc}(y,z,t)}{\partial y}\,@y=0 \tag{13}$$

Table 1. Geometric and Thermal Parameters used in the Simulations

Parameter	Value
Length of the channel (L)	10 cm (each)
Half wall thickness (ceramic) ($\delta_{c,wall}$)	88.5 μm
Half wall thickness (metallic) ($\delta_{m,wall}$)	25 μm
Thickness of the washcoat (δ_{wc})	30 μm
Effective transverse length scale(R_Ω)	264 μm
Density of gas at 298 K, 1 atm (ρ_f)	1.184 kg/m^3
Density of ceramic wall($\rho_{c,wall}$)	1675 kg/m^3
Density of metallic wall($\rho_{m,wall}$)	7500 kg/m^3
Density of washcoat (ρ_{wc})	1369 kg/m^3
Heat capacity of gas at 298 K($C_{p,f}$)	1005 J/kg.K
Heat capacity of ceramic wall($C_{p_{c,wall}}$)	1045 J/kg.K
Heat capacity of metallic wall($C_{p_{m,wall}}$)	460 J/kg.K
Heat capacity of washcoat ($C_{p,wc}$)	880 J/kg.K
Thermal conductivity of ceramic wall ($k_{c,wall}$)	1 W/mK
Thermal conductivity of metallic wall ($k_{m,wall}$)	40 W/mK
Thermal conductivity of washcoat (k_{wc})	1.5 W/mK

$$\frac{\partial X_{j,wc}(y,z,t)}{\partial y}=0 \qquad @y=\delta_c \tag{14}$$

$$X_{j,m}(z,t)=X_{\text{inlet}}(t) \qquad @z=0 \tag{15}$$

$$T_f(z,t)=T_{f\text{inlet}}(t) \qquad @z=0 \tag{16}$$

Properties of the LNT and SCR such as the cell density, channel length, and washcoat thickness are assumed to be uniform. The dependence of gas density (ρ_f), and average velocity ($\bar{u}$), on the temperature is taken into account through the continuity and ideal gas equations. The simulations were conducted using the following values: the total length of either the LNT or SCR catalyst (L) is 10 cm, the gas velocity at the inlet ($\bar{u}$) 9.8 m/s (gas hourly space velocity of ~120,000 h^{-1} at S.T.P. conditions or ~224,175 h^{-1} at 510 K, 1 atm and based on the total volume of the catalyst brick), hydraulic diameter ($4R_\Omega$) 1.105×10^{-3} m and washcoat thickness (δ_{wc}) of 3.0×10^{-5} m.

LNT Kinetic model

The NO_x storage and reduction catalyst considered in this study is $Pt/BaO/Al_2O_3$. The catalyst composition consists of 2.2 wt % Pt (21.9% Pt dispersion) and 16.3 wt % BaO deposited on Al_2O_3 washcoat. The kinetic model of the LNT catalyst accounts for the following reactions (a) NO oxidation to NO_2 on the precious metal, (b) storage of NO_2 in the form of nitrates or nitrites, and (c) reduction of stored NO_x with H_2 during the rich phase in the presence of O_2. The global kinetic mechanism used in this work is derived from Bhatia et al.[16] which considers fast (*f*) and slow (*s*) storage sites as described in the previous section

R1: $NO+\frac{1}{2}O_2 \rightleftharpoons NO_2 \qquad \Delta H_R=-57.2\frac{kJ}{\text{mol. }NO}$

R2: $3NO_2+BaO(f) \rightarrow Ba(NO_3)_2(f)+NO \qquad \Delta H_R=-149.2\frac{kJ}{\text{mol. }NO_2}$

R2a: $\theta_v(f)+\theta_{Ba(NO_3)_2}(f)=1$ (fast sites)

R3: $3NO_2+BaO(s) \rightarrow Ba(NO_3)_2(s)+NO$

R3a: $\theta_v(s)+\theta_{Ba(NO_3)_2}(s)=1$ (slow sites)

We consider that the rich feed consists of H_2 as a reducing agent which converts stored NO_x to NH_3 and N_2, thus, producing H_2O. Because of the presence of O_2 in the rich phase, part of the H_2 is converted to H_2O by the combustion reaction. Some of the NH_3 formed during the regeneration subsequently reacts with the stored NO_x to produce N_2. The regeneration is described by the following global reactions

R4: $8H_2+Ba(NO_3)_2(f) \rightarrow 5H_2O+BaO(f)+2NH_3 \qquad \Delta H_R=-135.3\frac{kJ}{\text{mol }.H_2}$

R5: $8H_2+Ba(NO_3)_2(s) \rightarrow 5H_2O+BaO(s)+2NH_3$

R6: $\frac{10}{3}NH_3+Ba(NO_3)_2(f) \rightarrow 5H_2O+BaO(f)+\frac{8}{3}N_2 \qquad \Delta H_R=-251\frac{kJ}{\text{mol }.NH_3}$

R7: $\frac{10}{3}NH_3+Ba(NO_3)_2(s) \rightarrow 5H_2O+BaO(s)+\frac{8}{3}N_2$

R8: $H_2O+X \rightleftharpoons H_2O-X$

Table 2. Kinetic Parameters used for LNT

k	A	E_a (kJ/ mol)
k_{f1}	7.5×10^{9}	0
k_{b1}	1.27×10^{16}	106.9
k_{f2}	6.81×10^{4}	0
k_{b2}	8.41×10^{12}	80
k_{f3}	4.5×10^{14}	101.3
k_{b3}	2.5×10^{14}	44.9
k_{f4}	8×10^{9}	0
k_{b4}	5.7×10^{17}	97.9
k_{f5}	4.94×10^{18}	80
k_{b5}	1×10^{22}	209.4
k_2	2.44×10^{8}	50.0
k_3	1.7×10^{9}	76.7
k_4	1×10^{9}	60.0
k_5	1×10^{10}	80.0
k_6	2.7×10^{11}	85.0
k_7	1.6×10^{12}	102.5
k_{8f}	1×10^{8}	52.0
k_{8b}	1×10^{7}	80.0
k_{9f}	$2.\times10^{7}$	42.0
k_{9b}	4×10^{6}	73.5
Concentration of Storage sites:		
$C_{BaO}(f) = 6.62\times10^{1}$ mol/m^3 washcoat		
$C_{BaO}(s) = 2.72\times10^{2}$ mol/m^3 washcoat		
$C_x = 96.7$ mol/m^3 washcoat		

Units of k or A depend on rate expression and are given in Appendix A1 online in Supporting Information

R9: $NH_3+X \rightleftharpoons NH_3-X$

R9a: $\theta_{H_2O,X}+\theta_{NH_3,X}+\theta_{v,X}=1$

here $\theta_{H_2O,X}, \theta_{NH_3,X}$ are the coverages of H_2O and NH_3 on Al_2O_3 sites, respectively and $\theta_{v,X}$ is the vacant site coverage. The heat generated due to R8 and R9 are negligible and not considered in the calculations. The rate expressions of the above reactions are reported in the Appendices A1 and A2. The kinetic parameters of the regeneration reactions are reported in Table 2. The microkinetic sequence that accounts for the reaction between NO and H_2 during the rich period and the corresponding rate constants are derived from the work of Xu et al.[17] The heat of reactions can be calculated from the activation energies listed in their work

R10: $NO+Pt \rightleftharpoons NO-Pt$

R11: $H_2+2Pt \rightleftharpoons 2H-Pt$

R12: $NO-Pt+H-Pt \rightleftharpoons N-Pt+OH-Pt$

R13: $H-Pt+O-Pt \rightleftharpoons OH-Pt+Pt$

R14: $H-Pt+OH-Pt \rightarrow H_2O+2Pt$

R15: $2N-Pt \rightarrow N_2+2Pt$

R16: $NO-Pt+Pt \rightleftharpoons N-Pt+O-Pt$

R17: $N-Pt+3H-Pt \rightleftharpoons NH_3-Pt+3Pt$

R18: $NH_3+Pt \rightleftharpoons NH_3-Pt$

R19: $O_2+2Pt \rightleftharpoons 2O-Pt$

SCR Kinetic model

The global kinetic model of the SCR reactions used in this work was originally developed for Cu-ZSM5 catalyst by Olsson et al.[18] The composition and site concentration of Cu is similar to that used in their work. The model accounts for

Table 3. Kinetic Parameters used for SCR

k	A	E_a (kJ/mol)
k_{20f}	9.3×10^{-1}	0
k_{20b}	1.0×10^{11}	$181.5\times(1 - 0.98\ \theta_{NH_3})$
k_{21}	1.2×10^{11}	162.4
k_{22f}	8×10^{1}	48[a]
k_{23}	2.3×10^{8}	84.9
k_{24}	1.9×10^{12}	85.1
k_{25}	1.1×10^{7}	72.3
k_{26}	3.6×10^{4}	43.3

a) k_{22b} is calculated from thermodynamic constraints.
$C_s = 3939.4$ moles/m^3 washcoat

Units of k or A depends on rate expression and is given in Appendix A3 online in Supporting Information

NH_3 adsorption, NO oxidation to NO_2, selective reduction of NO_x by adsorbed NH_3, NH_3 oxidation, and a side reaction producing N_2O. The kinetic model assumes an Eley-Rideal mechanism to account for the reaction between adsorbed NH_3 and gas phase NO_x.[19] The reactions considered in the NH_3 SCR are

R20: $NH_3+S \rightleftharpoons NH_3-S \quad \Delta H_R=-181.5\frac{kJ}{mol.NH_3}@\theta_{NH_3}=0$

R21: $2NH_3-S+\frac{3}{2}O_2 \rightarrow N_2+3H_2O+2S \quad \Delta H_R=-130\frac{kJ}{mol.NH_3}$

R22: $NO+\frac{1}{2}O_2 \rightleftharpoons NO_2 \quad \Delta H_R=-57.2\frac{kJ}{mol.NO}$

R23: $4NH_3-S+4NO+O_2 \rightarrow 4N_2+6H_2O+4S \quad \Delta H_R=-226\frac{kJ}{mol.NH_3}.$

R24: $2NH_3-S+NO+NO_2 \rightarrow 2N_2+3H_2O+2S \quad \Delta H_R=-197\frac{kJ}{mol.NH_3}.$

R25: $4NH_3-S+3NO_2 \rightarrow 3.5N_2+6H_2O+4S \quad \Delta H_R=-160\frac{kJ}{mol.NH_3}$

R26 :$2NH_3-S+2NO_2 \rightarrow N_2+N_2O+3H_2O+2S \quad \Delta H_R=-192\frac{kJ}{mol.NH_3}$

R27:$\theta_v+\theta_{NH_3}=1$

The rate expressions for these reactions and the corresponding kinetic parameters are reported in Appendix A3 (see online in Supporting Information), and Table 3, respectively. Heats of reaction are calculated based on gas phase NH_3 and subtracting the heat of adsorption from that of the reaction.

Characteristic Times and Front Speeds

The qualitative dynamic features of the reactor can be predicted by inspection of the characteristic times $\tau_c(=L/\bar{u}), \tau_D\left(=R_\Omega^2/D_{m,j}\right), \tau_{WD}\left(=\delta_{wc}^2/D_{e,wc}\right), \quad \tau_{R_j}\left(=C_{ref}/R\left(C_{ref}\right)\right)$ in the LNT and SCR for convection, external mass transfer, washcoat diffusion (internal mass transfer) and reactions, respectively. These values are reported in Table 4 at 510 K and at 573 K. We chose these two temperatures because the average temperature rise in the monolith under aerobic operation is $\sim$ 60 K in our base case study and $\sim$ 5 K under anaerobic operation. The characteristic times of both the LNT and SCR reactions decrease when the temperature increases from 510 K to 573 K. The increased rates of storage and regeneration on slow sites, NH_3 regeneration and standard SCR reactions significantly increase the NO_x conversion. Table 4 shows that the temperature rise increases the ratio between the convection to the slow storage times from 0.18 to 1.20, which indicates that the NO_x slip during the lean period has been reduced. The time constants reveal that the aerobic operation has a stronger impact on the NO oxidation reaction than on the slow storage reaction. This increases the ratio of exit NO_2/NO from the LNT which is desirable since it improves the efficiency of the SCR downstream. Otherwise, the ratio of exit NO_2/NO is less than one due to washcoat diffusional limitations, unlike that reported for the isothermal case,[11] in which washcoat diffusion was not considered. Also the diffusion time within the washcoat indicates that NO_x storage and H_2 regeneration reactions on fast sites are limited by washcoat diffusion even at 510 K. The generalized Thiele modulus ($\phi_w^2=\frac{\tau_{WD}}{\tau_R}$) is greater than one for these reactions indicating that washcoat diffusional resistance exists. As the brick temperature increases, NH_3 regeneration reactions (R6 and R7) in the LNT are limited by the diffusional resistance, as a result more NH_3 enters into the SCR.

During the lean period the NO in the feed is oxidized to form NO_2 which is then stored on the BaO storage sites to form $Ba(NO_3)_2$. The propagation speed of the storage front can be predicted by the relation[20]

$$u_{c,str}=\frac{\bar{u}R_\Omega C_{NO}^{in}}{3\delta_{wc}C_{BaO(f)}^{\circ}} \tag{18}$$

where $\bar{u}$ is the gas velocity, R_Ω is the effective transverse length scale, is the inlet NO concentration, δ_c is the washcoat thickness, $C_{BaO(f)}^{\circ}$ is the NO_x storage capacity on fast sites. The aforementioned expression is valid when washcoat diffusional resistance is negligible and the storage is in the mass transfer limited regime. The speed of the fast site storage front is $\sim$ 5.4 mm/s. Since the regeneration time of the stored NO_x by H_2 $\left(\tau_{R_4}=\frac{C_{ref}}{R_V\left(C_{ref}\right)}\right)$ is faster than that by NH_3, the speed of propagation of the regeneration front can be calculated by the expression[20]

$$u_{c,reg}=\frac{\bar{u}R_\Omega C_{H_2}^{in}}{8\delta_{wc}C_{BaO(f)}^{\circ}} \tag{19}$$

which is 36 mm/s during aerobic reduction (with 1.875% H_2), and 16.8 mm/s during anaerobic reduction (0.875% H_2).

Table 4. Estimated Characteristic Times of Different Processes in the LNT Catalyst

Characteristic time (ms)	Temperature (K)	
	510	573
τ_C	10.2	9.10
τ_D	1.46	1.19
τ_{WD}	4.40	4.10
τ_{R_1}	8.75	0.82
τ_{R_2}	0.50	0.10
τ_{R_3}	56.0	7.50
τ_{R_4}	1.40	0.21
τ_{R_5}	15.0	1.80
τ_{R_6}	14.0	1.60
τ_{R_7}	52.0	3.40

Table 5. Estimated Characteristic Times of Different Processes in the SCR Catalyst

Characteristic time (ms)	Temperature (K)	
	510	573
τ_C	10.2	9.10
τ_D	1.46	1.19
τ_{WD}	4.40	4.10
$\tau_{R_{23}}$	359.7	42.7
$\tau_{R_{24}}$	7.60	0.81
$\tau_{R_{25}}$	385.0	60.0

Again, the aforementioned speeds of the storage and regeneration fronts are of the fast sites in the LNT and when washcoat diffusional resistance is negligible.

During the rich phase H_2 is fed into the reactor in the presence of O_2 to regenerate the BaO sites that store the NO_x. H_2 reacts with the O_2 and spilled over NO_x from the storage sites on to the Pt sites. The released reaction heat raises the monolith temperature forming a temperature front that propagates along the reactor. In general, the speed of this temperature front does not have to be equal to the speed of the regeneration front due to different storage and thermal capacities of the monolith channel, especially for long channels or when there are excursions in inlet temperatures (leading to pure thermal waves). For the parameters considered in this study, the light off occurs in the upstream of the monolith channel and the thermal front propagates downstream. The propagation speed of the thermal front (for the case of long channels where the axial conduction effects can be neglected) can be estimated by the expression[21]

$$u_{t,f} = \bar{u}\left(\frac{\rho_f C_{p,f}}{\rho_s C_{p,s}}\right)\left(\frac{R_\Omega}{\delta_s}\right) \tag{20}$$

Here, $\bar{u}$ is the average gas velocity in the channel, $\left(\frac{\rho_f C_{p,f}}{\rho_s C_{p,s}}\right)$ is the fluid to solid heat capacitance ratio, (R_Ω/δ_s) is the ratio of effective transverse length scale of the bulk fluid phase to the solid phase. For the values given in Table 1 the speed of the thermal front is estimated to be ~10 mm/s, and the thermal front propagation time in the LNT (with L = 10 cm) is ~10 s.

In the case of a one-step exothermic reaction on identical sites, the speeds of the regeneration and temperature fronts are equal. It follows from the front speed estimates that for the geometrical, thermal properties and the inlet concentrations considered for the model, the regeneration front speed is higher than that of the thermal or storage fronts. An estimate of the front speeds provides insight into the overall operation of the system. For example, from the storage front speed, we note that in a 10 cm long LNT, all the fast sites are occupied in about 18.5 s. Similarly, if the inlet gas temperature (during the rich pulse) is different from the monolith temperature during the rich period, most of the regeneration reactions are completed even without any significant increase in the temperature. Although the average temperature over the lean cycle increases due to adiabatic operation, the effect is moderate because of the rapid cooling front that travels along the LNT. The LNT—SCR catalyst sequence should be designed so that the storage takes advantage of the travelling temperature wave. Later we present simulations under aerobic (with O_2 during the rich phase) and anaerobic (no O_2 during the rich phase) conditions, directed to optimize the design and operation of the sequence of the LNT and SCR catalyst system. We study the impact of Pt loading, cycle time, length of the catalyst, nature of the support material and catalyst architecture on the performance of the combined system.

Results and Discussion

Effect of Pt loading on fuel penalty

The sequential system of the LNT and SCR is operated periodically with 60 s lean feed followed by 10 s rich feed. The length of each catalyst in the base case is taken to be 10 cm and the same gas hourly space velocity (GHSV) was maintained under anaerobic and aerobic conditions. Extended channel length enables us to analyze the impact of traveling temperature fronts which may not be formed in the short channels used in the laboratory studies. The lean feed contains 500 ppm NO and 5% O_2, while the rich feed contains 500 ppm NO, 1.875% H_2, and 0.5% O_2. The inlet gas velocity, inlet and initial temperatures are correspondingly 9.8 m/s and 510 K. The dependence of the kinetic parameters on the Pt loading is accounted for by the expression

$$k_i = k_B\left(C^i_{Pt}/C^B_{Pt}\right)^m. \tag{21}$$

Here, C^i_{Pt} is the desired catalyst Pt loading in mol/m^3 of washcoat, C^B_{Pt} is the Pt loading with known kinetic parameters (k_B), m is the sensitivity of the kinetic parameters on the Pt loading. Xu et al.[22] have shown that $m = 1$ adequately predicted their experiments using a catalyst composition similar to that used in the current study. We refer to their work for a detailed analysis of m.

It has been suggested that a sequence of the LNT—SCR catalysts enables a reduction of the NO_x emission and the NH_3 slip.[14,15] Figure 1 compares the cycle averaged NO_x conversions obtained using a sequential LNT—SCR system with 2.2 and 0.2 wt % Pt loading under both anaerobic and aerobic conditions. The simulations show that aerobic reduction of NO with reduced Pt loading results in higher NO_x conversion than that of a base case anaerobic operation. The kinetics of both the storage and regeneration reactions is enhanced due to the adiabatic temperature rise resulting from the H_2 oxidation by O_2. The average temperature of the catalyst is higher under aerobic conditions. Temperature profiles during both the lean and rich periods are shown in Figure 2. The NO_x conversion obtained with 2.2 wt % Pt under anaerobic condition is slightly lower than that obtained under aerobic operation with 0.2 wt % Pt loading. Excess reductant, that is, fuel penalty is required to obtain the needed average temperature rise of the catalyst. A fuel penalty of 1% H_2 during the 10 s lean feed is 0.14% for a total cycle time of 70 s. Increasing the fuel penalty increases the NO_x conversion as shown in Figure 3. However, the impact of the increase is small for a fuel penalty exceeding 0.43% due to washcoat diffusion and external mass-transfer

Table 6. Temperature-Dependent Diffusivities of Gas Species

Species	$D_{m,j}$ (m^2/s)
NO	$1.33\times10^{-9} \times T^{1.696}$
NO_2	$0.8 \times 10^{-9} \times T^{1.7037}$
O_2	$1.336 \times 10^{-9} \times T^{1.6942}$
H_2	$5.8 \times 10^{-9} \times T^{1.6657}$
N_2	$1.34 \times 10^{-9} \times T^{1.6901}$
NH_3	$1.215 \times 10^{-9} \times T^{1.7389}$
H_2O	$0.95 \times 10\text{-}9 \times T^{1.7778}$

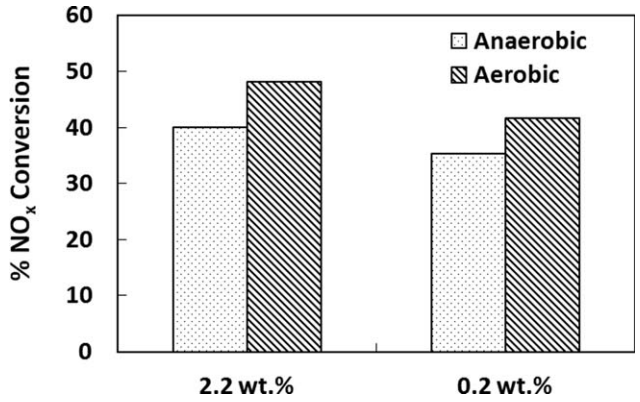

Figure 1. Impact of Pt loading and nonisothermal effects on cycle averaged NO_x conversion by a pair of LNT - SCR catalysts. [$T_{in} = T_{initial} = 510$ K, $L_{LNT} = L_{SCR} = 10$ cm, $\bar{u} = 9.8$ m/s (inlet), $t_L = 60$ s, $t_R = 10$ s].

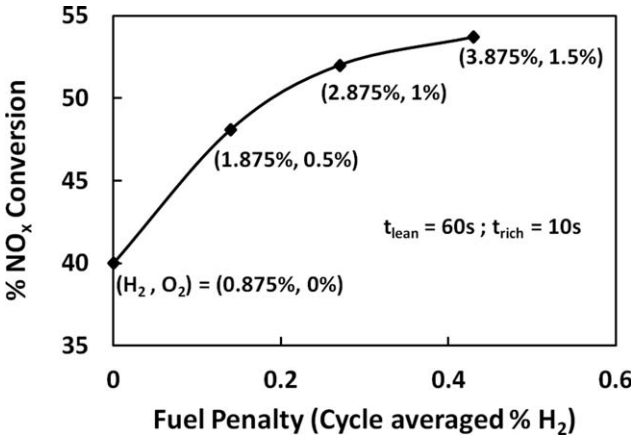

Figure 3. Effect of fuel penalty on NO_x conversion in the sequence of LNT-SCR catalysts. [(% H_2, % O_2) represents the concentration of H_2 and O_2 during the rich phase].

limitations which become dominant at higher reaction rates. The results indicate that it is possible to reduce the precious metal loading under aerobic operation by use of excess H_2. However, a significant reduction in the Pt loading can increase the ignition time and hence the fuel penalty and may decrease the catalyst durability, because of catalyst deactivation at very low Pt loading.

Effect of cycle time

The cycle time is one of the key parameters that affect the performance of monolith reactors. It can be changed by variation of either the lean or the rich period or both. Previous studies[23–25] have shown that the NO_x conversion increases as the total cycle time is shortened at a fixed ratio of the lean to rich period (i.e., at a fixed pulse duty, which is the ratio of the rich period to the total cycle time). We have performed simulations that include changing the total cycle time and also the pulse duty. Figures 4 and 5 show the impact of changing the total cycle time as well as of the pulse duty. Here we compare the anaerobic and aerobic NO_x conversion for total cycle times of 70 s (pulse duty $= t_R/(t_L + t_R) = 1/7$), 40 s ($t_R/(t_L + t_R) = 1/4$), and 20 s ($t_R/(t_L + t_R) = 1/4$). An increase in the pulse ratio, i.e., the fraction of the cycle time with a rich feed, increases the cycle averaged NO_x conversion. The reason is that, it leads to a higher temperature during the lean period, thereby increasing the rates of the NO oxidation and storage. During the 70 s cycle, a high-temperature wave exists for only 10 s during lean phase as evident from the propagation of the thermal and concentration fronts. This high temperature wave exists only for ~16% of the lean period. However, during the 40 s cycle a high-temperature wave exists for ~33% of the lean period.

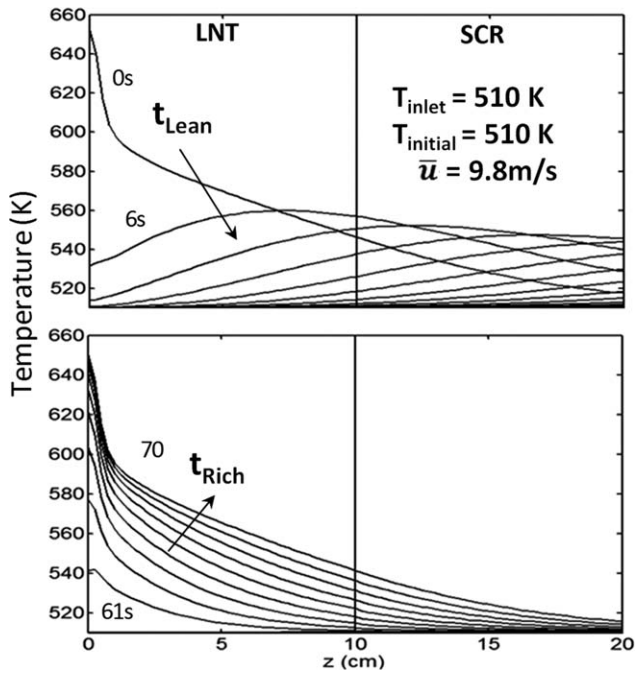

Figure 2. Catalyst temperature profiles during lean and rich periods with $t_{Lean} = 60$ s and $t_{Rich} = 10$ s.

The NO_x conversion can be increased by decreasing the total cycle time. This behavior is expected because of the increased regeneration frequency. Fast sites are quickly saturated when compared to slow sites. As the total cycle time is reduced, most of the storage and regeneration processes take place on fast sites without any significant usage of slow sites. This results in reduced NO_x slip from the LNT. The average temperature rise does not change when the pulse duty is changed, but it increases when the total cycle time is decreased at a fixed pulse duty. The higher conversion in the latter case occurs because of both the increase in regeneration frequency and higher average temperature.

Effect of catalyst length

Figure 6 compares the NO_x conversion of the base case (with 10 cm each of LNT and SCR) with those for other catalyst lengths, i.e., 4 cm, 2 cm, and 1 cm each. The residence time is approximately same in all these cases. The corresponding effective heat Peclet number is defined as[26]

$$\frac{1}{Pe_{h,eff}} = \frac{1}{Pe_h} + \frac{R_\Omega^2 \bar{u} \rho_f C_{p,f}}{k_f L Nu_\Omega} \tag{22}$$

where Nu_Ω is the Nusselt number, is the thermal conductivity of the gas phase. The solid (or intraphase) heat Peclet number $Pe_h = \frac{\bar{u} L \rho_f C_{p,f} R_\Omega}{\delta_s k_s}$ varies from 14.56 to 1456.3 as the catalyst length is increased from 1 cm to 10 cm. The first

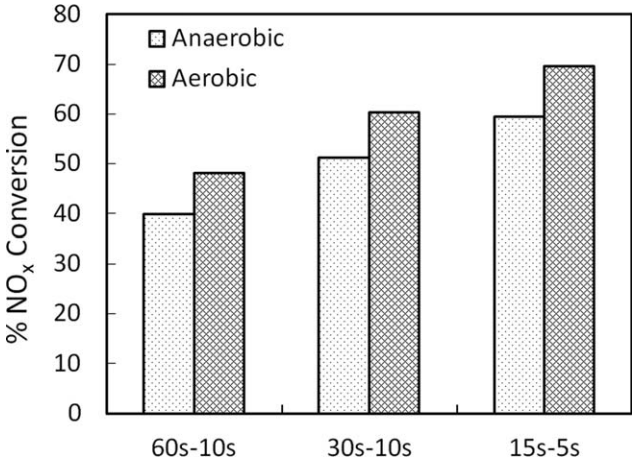

Figure 4. Impact of total of cycle time on time averaged NO_x conversion by aerobic reduction by a pair of LNT - SCR. [$T_{in} = T_{initial} = 510$ K, $L_{LNT} = L_{SCR} = 10$ cm, $\bar{u} = 9.8$ m/s (inlet), Pt = 2.2 wt %].

term on the righthand side of Eq. 22 represents intraphase heat transfer, and second, the interphase heat transfer. For the parameters considered, the second term dominates the mode of heat transfer and the temperature rise in the solid phase is mainly due to heat exchanged from the gas. Figure 6 shows the dependence of NO_x conversion on catalyst length during aerobic operation and is representative of the variation of heat-transfer modes with the aspect ratio. We observed small difference in the NO_x conversion due to the high-space velocity considered in this study. However, the effect of varying heat-transfer modes with the aspect ratio is discernible. Interphase heat transfer being the dominant mode causes a rapid cooling during the start of the lean cycle for long catalysts, as shown in Figure 7. Decreasing the length (and linear velocity) shifts the heat-transfer mode in the catalyst from interphase to intraphase mode. When the intraphase term is significant in Eq. 22, the solid conduction disperses the heat generated in the washcoat along the catalyst length. The combined effect results in an optimum

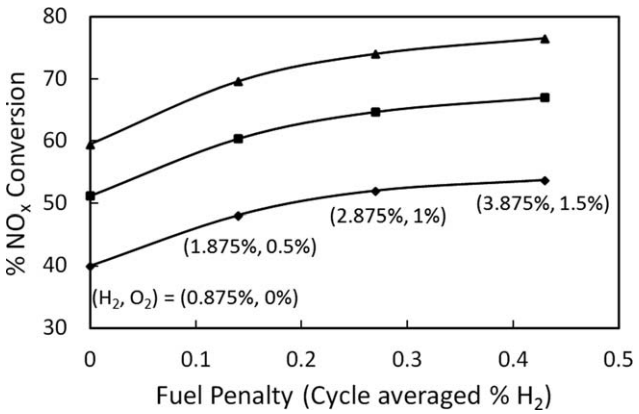

Figure 5. Impact of total of cycle time and fuel penalty on time averaged NO_x conversion under aerobic operation by a pair of LNT - SCR. [$T_{in} = T_{initial} = 510$ K, $L_{LNT} = L_{SCR} = 10$ cm, $\bar{u} = 9.8$ m/s (inlet), Pt = 2.2 wt %; $t_{lean} = 60$ s (◆), 30 s (■), 15 s (▲); $t_{rich} = 10$ s (◆), 10 s (■), 5 s (▲)].

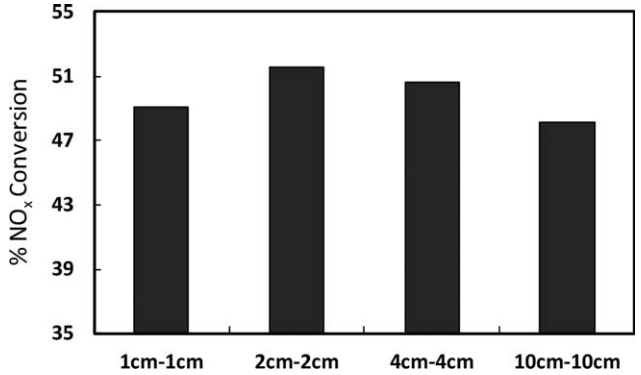

Figure 6. Comparison of cycle averaged NO_x conversion by a pair of LNT-SCR for different lengths of the catalyst during aerobic operation.

length that retains heat in the catalyst for a longer period resulting in enhanced reaction rates. As the length of the catalyst is further decreased (1 cm or lower), intraphase heat transfer becomes the dominating mode and also there is a significant decrease in temperature rise at the inlet. Hence, the NO_x conversion for 1 cm catalyst is lower than that of 2 cm. This explains the different performance of catalysts with different lengths, which is not present during anaerobic operation. It should be noted that this effect could be more significant when the space velocity is decreased. We choose a high-space velocity in this study to focus on a base case with low NO_x conversion so that any increase based on the parameters studied can be appropriately noted.

Effect of the support material

Few studies compared the performance of exhaust gas after-treatment systems using metallic monoliths with those using ceramic monoliths. Nishizawa et al.[27] have concluded that metallic monoliths lead to a higher conversion than ceramic monoliths. Pfalzgraf et al.[28] reported that the type of support material does not affect the performance of the converter. Santos and Costa[29] have concluded that the metallic converters perform well at high-space velocities and the ceramic at low-space velocities. Gundlapally and Balakotaiah[26] have performed a detailed analysis of the steady state behavior of both metallic and ceramic converters and concluded that for a low-transverse heat Peclet number $\left(P_h = \frac{R_\Omega^2 \bar{u} \rho_f C_{pf}}{L k_f}\right)$ ceramic converters perform better while at high-transverse Peclet number metallic converters perform better. Our simulations (Figure 8) have shown that the LNT—SCR sequence with a metallic support perform marginally (~2%) better than those with a ceramic support. Due to high-gas velocity and high conductivity of the metal support both the convection and conduction modes of heat transfer contribute to the increase in NO_x conversion. Also, the temperature profiles are broader than those in a ceramic support. The ratio between the heat capacities of the ceramic and metallic monoliths is estimated to be 1.56, and the temperature front propagation time in the metallic monolith is ~ 0.6 times of that in the ceramic monolith. For low-space velocity operation of the combined catalyst, large differences in the performances of metallic and ceramic monoliths are expected because of the variation in the dominant heat transfer mode as described earlier.

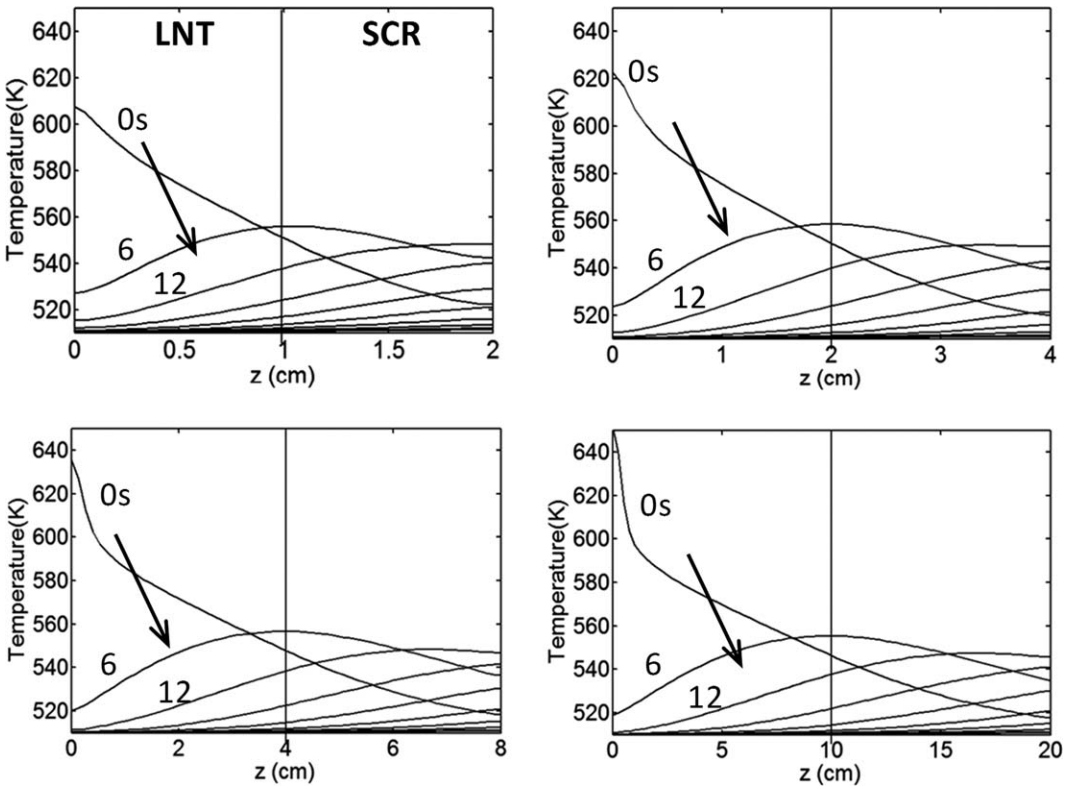

Figure 7. Catalyst temperature profiles for different lengths of LNT-SCR catalysts during the lean feed. [$T_{in} = T_{initial} = 510$ K, $\bar{u} = 9.8$ m/s (inlet), Pt = 2.2 wt %, $t_{Lean} = 60$ s, $t_{Rich} = 10$ s].

Effect of catalyst architecture

We study the impact of using n LNT–SCR catalysts of equal length ("n" being the number of LNT—SCR catalyst pairs). Figure 9 is a schematic description of several sequences of LNT–SCR catalysts ($n = 1$, $n = 2$ and $n = 4$). The LNT catalyst is the first one in each sequence and the total length of the catalyst is the same in all cases. This architecture decreases the NH_3 reaction in the LNT and stores it in the adjacent SCR. This reduces NO_x slip out of the LNT during the subsequent lean period. Experiments on similar architectures[9,10] verified that the NO_x conversion can be increased by a sequence of LNT and SCR catalysts. Similar results are predicted by our model during aerobic operation, as shown in Figure 10. Due to the fast H_2 oxidation, all the oxygen is consumed in the first LNT catalyst. Thus, except for the first catalytic zone the temperature rise downstream is mainly due to the convective heat transfer. This suggests that the only advantage of using multiple zones under aerobic operation is the increase in the average temperature of the monolith.

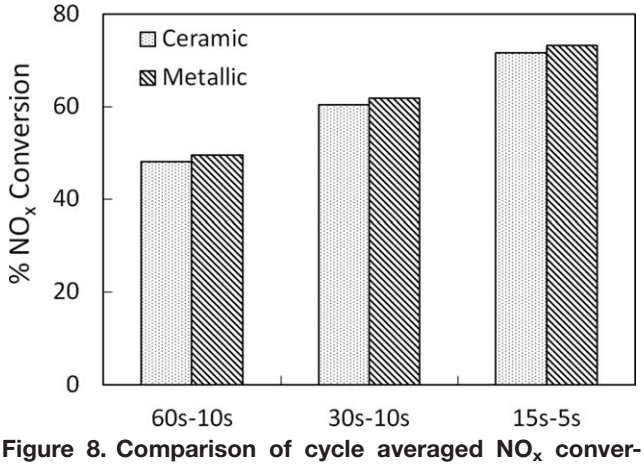

Figure 8. Comparison of cycle averaged NO_x conversion by a pair of LNT-SCR using either a ceramic or metallic support.

Effect of nonuniform PGM loading

Pt loading profile is one of the key parameters that can optimize the performance of the combined LNT—SCR

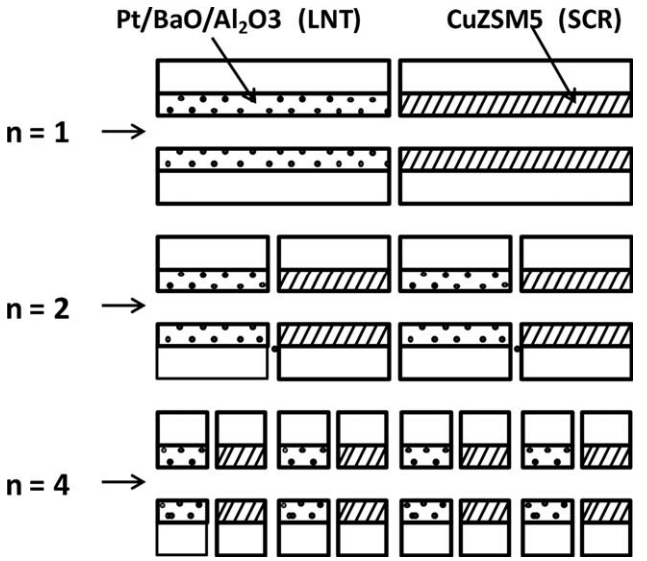

Figure 9. Schematic arrangement of the sequential pairs of LNT-SCR catalysts.

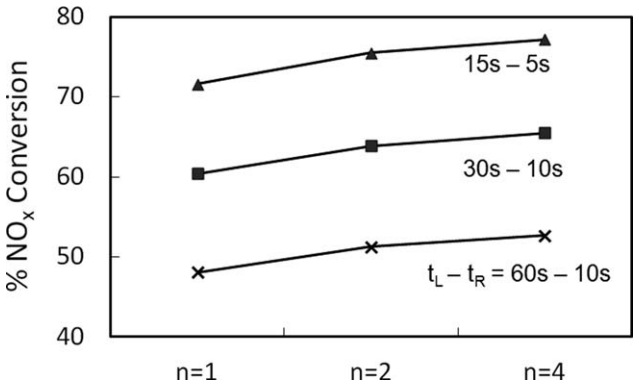

Figure 10. Comparison of cycle averaged NO_x conversion during aerobic operation using sequential LNT - SCR pairs with n = 1, 2 and 4 architecture. [$T_{in} = T_{initial} = 510$ K, $L_{LNT} = L_{SCR} = 10$ cm, $\bar{u} = 9.8$ m/s (inlet), Pt = 2.2 wt %].

system. Under isothermal conditions Kota et al.[11] have shown that nonuniform Pt loading in equal sized LNT and SCR catalysts improved the NO_x conversion following a decrease of the Pt loading in the first LNT catalyst and shifting it to the second LNT catalyst. This enhanced the NH_3 selectivity in the first LNT and increased the NO_x conversion in the second. However, additional decrease of the Pt loading may deteriorate the system performance. We conducted two simulations of similar LNT and SCR catalyst sequence, using a detailed model that accounts for the washcoat diffusion. One with lower Pt loading (1.32 wt % and 0.44 wt %) in the front and higher (3.08 wt % and 3.96 wt %) in the back LNT catalyst. Both downstream loadings decreased the conversion over that obtained with uniform loading as shown in Figure 11a. The second simulation is of the inverse loading policy with a higher loading in the first LNT and lower in the second. Figure 11b shows that the cycle averaged NO_x conversion was higher than that under uniform loading. When more Pt is loaded in the downstream catalyst, the first LNT catalyst does not fully benefit from the temperature rise due to the H_2 oxidation because of the low Pt loading. However, when the Pt loading in the first LNT is high both the storage and regeneration kinetics are significantly enhanced and the NO_x conversion is increased.

Impact of washcoat diffusion

Simulations were performed for the operating conditions selected, to assess the impact of the washcoat diffusion on the cycle averaged NO_x conversion. The effective diffusivities of the species have been artificially increased in some simulations to eliminate the washcoat diffusional resistance. Figure 12 shows that the cycle averaged NO_x conversion is higher when no washcoat diffusion exists under both aerobic and anaerobic operation. The diffusional resistance diminishes the NO_x conversion by $\sim$ 20%. This is because at high-temperatures fast reactions like NO_x storage and H_2 regeneration on fast sites are limited by washcoat diffusion. The impact of washcoat diffusional resistance increases as the total cycle time is reduced, because only fast sites are involved in the storage and regeneration chemistry. Increasing the fuel penalty increased the reaction rates due to the higher average temperature of the monolith. However, the NO_x conversion slowly approaches an asymptotic limit due

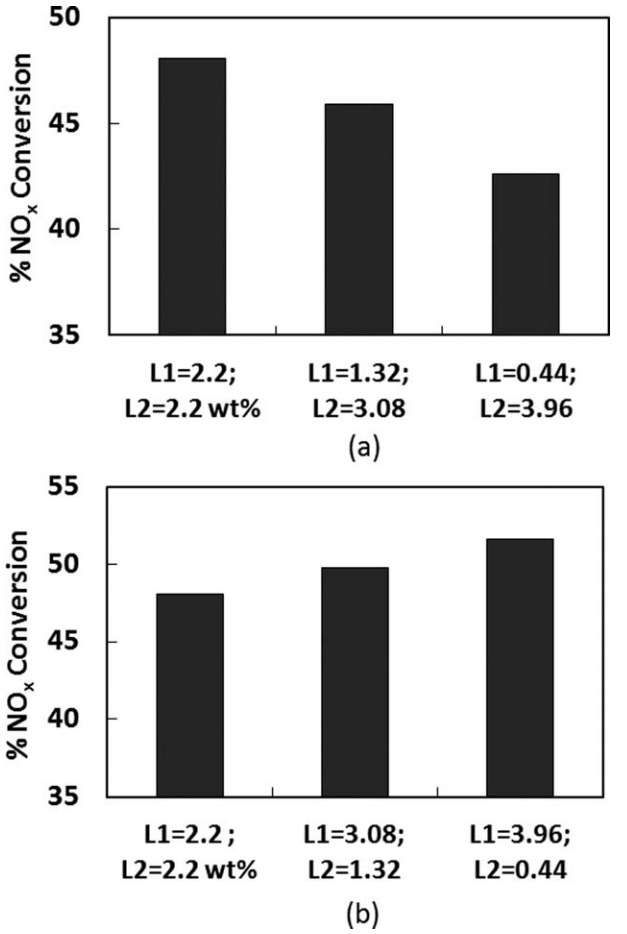

Figure 11. Comparison of cycle averaged NO_x conversion in a sequential LNT - SCR system with n = 2 architecture. Nonuniform Pt loading effect [$T_{inlet} = T_{initial} = 510$ K, $L_{LNT} = L_{SCR} = 10$ cm, $\bar{u} = 9.8$ m/s (inlet), L1 = first LNT, L2 = second LNT].

to the dominant washcoat diffusion and external mass-transfer limitations at high temperatures. Simulations indicate that it is important to account for the washcoat diffusional

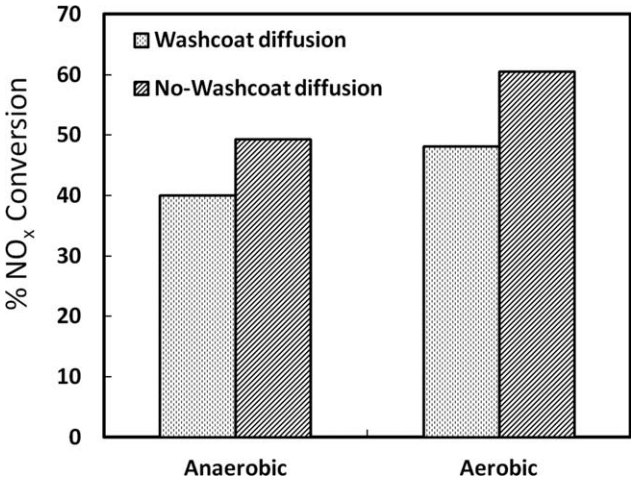

Figure 12. Impact of washcoat diffusion during anaerobic and aerobic operation. [$T_{in} = T_{initial} = 510$ K, $L_{LNT} = L_{SCR} = 10$ cm, $\bar{u} = 9.8$ m/s (inlet)].

effects in predictions of the performance of sequential LNT and SCR catalysts to avoid erroneous predictions of the cycle averaged NO_x conversion.

Conclusions

This study is focused on the adiabatic, aerobic operation of sequential LNT—SCR catalyst. We found that washcoat diffusional resistance, which is usually neglected, can be important in either anaerobic or aerobic operation, and it diminishes the reaction rates resulting in reduced conversions. For the same Pt loading and with other parameters considered in this work, the NO_x conversion using a sequence of LNT—SCR catalysts under aerobic operation exceeds that of the anaerobic operation by up to 10%. The simulations show that it is possible to reduce the precious metal loading under aerobic operation of the LNT—SCR catalyst sequence. The cycle time and pulse duties have a major impact on the overall NO_x conversion. For operating conditions considered in this study, decreasing the total cycle time (higher regeneration frequency) or increasing the pulse duty (longer time of exothermic reaction) increases the NO_x conversion by $\sim$ 41% over the anaerobic operation with the parameters considered in this work. The predicted increase of the NO_x conversion upon using the sequence of multiple LNT—SCR catalysts is similar to experimental observations reported in the literature.[9] Under aerobic operation the highest NO_x conversion is obtained when the LNT and SCR attain an intermediate catalyst length, which in our base case was 2 cm each. Hence, for a given NO_x conversion it is possible to reduce the amount of precious metal. Nonuniform Pt loading affects the NO_x conversion. With a high-upstream loading of precious metal in the LNT the conversion exceeds that of the uniform loading case. In contrast, a high-downstream loading decreases the conversion below that obtained with a uniform loading. Important observations are that the aerobic operation can significantly increase the NO_x conversion and could enable a decrease in the precious metal loading. However, such reduction in the precious metal loading should take into account the corresponding decrease in resistance to deactivation and the increase in the ignition time.

Acknowledgments

The senior authors dedicate this contribution to their distinguished teacher, mentor, role model and a continuous source of inspiration, late Professor Neal R. Amundson. This work was supported by the U.S. DOE National Energy Technology Laboratory (DE—FC26-05NT42630). This report was prepared as an account of work sponsored by an agency of United States Government. Neither the United States Government nor any agency thereof, nor any of their employees, makes any warranty, express or implied, or assumes any legal liability or responsibility for the accuracy, completeness, or usefulness of any information, or process, disclosed.

Notation

a = average pore radius inside the washcoat
A = pre-exponential factor (for units see Appendices provided in the Supporting Information)
$C_{BaO}(f,s)$ = total concentration of fast or slow BaO sites, mol of BaO/m^3 washcoat
$C_{Pt}^{\,i}$ = total platinum concentration of the catalyst, mol of Pt/m^3 washcoat
C_{ref} = reference concentration, mol/m^3
C_S = total concentration of NH_3 adsorption sites, mol/m^3 washcoat
C_{Tm} = total concentration in fluid phase, mol/m^3
C_x = concentration of adsorption sites for H_2O and NH_3 on Al_2O_3, mol/m^3 washcoat
$D_{m,j}$ = diffusivity of species j in gas phase, m^2/s
$D_{e,wc}$ = effective diffusivity of species j in washcoat, m^2/s
$k_c(j,z)$ = mass-transfer coefficient of species j at axial position z, m/s
k = reaction rate constant (for units refer to Appendices)
L = length of the monolith, m
m = sensitivity of the rate constant to Pt concentration
n = number of LNT—SCR zones
Nu_Ω = Nusselt number
P_h = transverse heat Peclet number
Pe_h = heat Peclet number
$Pe_{h,eff}$ = effective heat Peclet number
$R_{ad,j}$ = rate of adsorption of species j, mol/m^3washcoat/s
$R_{des,j}$ = rate of desorption of species j, mol/m^3washcoat/s
$R_{V,m}$ = rate of reaction m, mol/m^3washcoat/s
R_Ω = effective transverse length scale, m
t = time, s
T_f = gas-phase temperature, K
T_s = monolith temperature, K
$\bar{u}$ = average gas velocity in the fluid phase, m/s
$u_{c,str}$ = speed of propagation of storage front, m/s
$u_{c,reg}$ = speed of propagation of regeneration front, m/s
$u_{t,f}$ = speed of thermal front, m/s
$X_{j,m}$ = cup mixing mole fraction of species j
$X_{j,wc}$ = mole fraction of species j in washcoat
z = axial coordinate, m

Greek letters

α_v = platinum surface area per unit washcoat volume, m^2/m^3
δ_s = effective solid phase thickness, μm
δ_{wall} = half-wall thickness, μm
δ_{wc} = washcoat thickness, μm
ε_{wc} = porosity of washcoat
ρ_f = density of fluid phase, kg/m^3
ρ_{wall} = density of the wall, kg/m^3
ρ_{wc} = density of the washcoat, kg/m^3
$\theta_{Ba(NO_3)_2}$(f, s) = fractional surface coverage on fast or slow BaO sites occupied by NO_x
$\theta_{j,S}$ = fractional coverage of NH_3 adsorption sites on SCR catalyst
$\theta_{j,X}$ = fractional coverage of NH_3 and H_2O adsorption sites on Al_2O_3 support of LNT catalyst
θ_v (f,s) = fractional surface coverage of vacant fast or slow sites
τ_{R_j} = reaction time for the reaction j, s
τ = tortuosity factor
$\nu_{m,j}$ = stoichiometric coefficient of species j in reaction m
$\nu_{l,BaO}$ = stoichiometric coefficient in reaction l on fast or slow storage sites

Literature Cited

1. Muncrief RL, Khanna P, Kabin KS, Harold MP. Mechanistic and kinetic studies of NO_x storage and reduction on Pt/BaO/Al_2O_3. *Catal Today*. 2004;98:393–402.
2. Nova I, Lietti L, Forzatti P. Mechanistic aspects of the reduction of stored NO_x over Pt-Ba/Al_2O_3 lean NO_x trap systems. *Catal Today*. 2008;136:128–135.
3. Olsson L, Persson H, Fridell E, Skoglundh M, Andersson B. A kinetic study of NO oxidation and NO_x storage on Pt/Al_2O_3 and Pt/BaO/Al_2O_3. *J Phys Chem B*. 2001;105:6895–6906.
4. Koebel M, Elsener M, Kleemann M. Urea-SCR: a promising technique to reduce NO*x* emissions from automotive diesel engines. *Catal Today*. 2000;25:335–345.
5. Theis JR. A Lean NOx Trap + Selective Catalytic Reduction System for Controlling NOx Emissions from a Diesel Engine [Ph.D Dissertation]. Ann Arbor: University of Michigan; 2006.
6. Lindholm A, Sjövall H, Olsson L. Reduction of NO_x over a combined NSR and SCR system. *App Catal B Env*. 2010;98:112–121.

7. Forzatti P, Lietti L. The reduction of NO_x stored on LNT and combined LNT-SCR systems. *Catal Today*. 2010;155:131–139.
8. Seo CK, Kim H, Choi B, Lim MT. The optimal volume of a combined system of LNT and SCR catalysts. *J Ind Eng Chem*. 2011;17:382–385.
9. Gandhi HS, Cavataio JV, Hammerle RH, Cheng Y. Catalyst system for the reduction of NO_x and NH_3 emissions. US Patent: 7332135 B2, 2008.
10. Theis JR, Dearth M, McCabe R. LNT+SCR catalyst systems optimized for NO_x conversion on diesel applications. *SAE Technical paper*. 2011;01–0305.
11. Kota A, Luss D, Balakotaiah V. Modeling studies on Lean NOx reduction by a sequence of LNT-SCR Bricks. *Ind Eng Chem Res*. 2012;51:6686–6696.
12. Koltsakis GC, Haralampous OA, Koutoufaris IZ. Applications of multi-layer catalyst modeling in deNOx and DPF systems. *SAE Tech paper*. 2010;01–0893.
13. Chatterjee D, Koci P, Schmeißer V, Marek M, Weibel M, Krutzsch B. Modelling of a combined NO_x storage and NH_3-SCR catalytic system for diesel exhaust gas aftertreatment. *Catal Today*. 2010;151:395–409.
14. Ramanathan K, Balakotaiah V, West D H. Light-off criterion and transient analysis of catalytic monoliths. *Chem Eng Sci*. 2003;58:1381.
15. Mukadi LS, Hayes RE. Modelling the three way catalytic converter with mechanistic kinetics using the Newton-Krylov method on a parallel computer. *Comp Chem Eng*. 2002;26:439–455.
16. Bhatia D, Clayton RD, Harold MP, Balakotaiah V. A global kinetic model for NO_x storage and reduction on $Pt/BaO/Al_2O_3$ monolithic catalysts. *Catal Today*. 2009;147(1): S250.
17. Xu J, Clayton RD, Balakotaiah V, Harold MP. Experimental and microkinetic modeling of steady state NO reduction by H_2 on $Pt/BaO/Al_2O_3$ monolith catalysts. *App Catal B Env*. 2008;77:395–408.
18. Olsson L, Sjovall H, Blint RJ. A kinetic model for ammonia selective catalytic reduction over Cu-ZSM5. *Appl Catal B: Env*. 2008;81: 203–217.
19. Tronconi E, Nova I, Ciardelli C, Chatterjee D, Bandl-Konrad B, Burkhardt T. Modelling of an SCR catalytic converter for diesel exhaust after treatment: Dynamic effects at low temperature. *Catal Today*. 2005;105:529–536.
20. Clayton RD, Harold MP, Balakotaiah V. NO_x Storage and Reduction with H_2 on $Pt/BaO/Al_2O_3$ Monolith: Spatio-temporal resolution of product distribution. *Appl Catal B Env*. 2008;84:616–630.
21. Ramanathan K, Balakotaiah V, West DH. Optimal design of catalytic converters for minimizing cold start emissions. *Catal Today*. 2004;98:357–373.
22. Xu J, Harold MP, Balakotaiah V. Modeling the effects of Pt loading on NOx storage on Pt/BaO/Al2O3 catalysts. *Appl. Catal. B: Env*. 2011;104:305–315.
23. Sharma M, Harold MP, Balakotaiah V. Analysis of periodic storage and Reduction of NOx in catalytic monoliths. *Ind Eng Chem Res*. 2005;44:6264–6267.
24. Muncrief RL, Kabin KS, Harold MP. NO_x storage and Reduction with Propylene on Pt/BaO/Alumina. *AIChE J*. 2004a;50:2526–2540.
25. Kabin KS, Muncrief RL, Harold MP. NO_x Storage and reduction on Pt/Ba/Al2O3 monolithic storage catalyst. *Catal Today*. 2004;96: 79–89.
26. Gundlapally SR, Balakotaiah V. Effect of non-uniform activity and conductivity on the steady-state and transient performance of catalytic reactors. *Chem Eng Sci*. 2012; in review.
27. Nishizawa K, Masuda K, Horie H, Hirohashi J. Development of improved metal-supported catalyst. *SAE Tech Paper*. 1989. doi: 10.4271/890188.
28. Pfalzgraf B, Rieger M, Ottowitz G. Close coupled catalytic converters for compliance with LEV/ULEV and EG III legislation - influence of support material, cell density and mass on emission results. *SAE TechPaper*. 1996. doi:10.4271/960261.
29. Santos H, Costa M. Evaluation of the conversion efficiency of the ceramic and metallic three way catalytic converters. *Energy Conserv Manage*. 2008;49:291–300.

Manuscript received Nov. 29, 2012, revision received Apr. 5, 2013, and final revision received Jun. 10, 2013.